Analytical and Finite Element Study for Optimal Strain Distribution in Various Beam Shapes for Energy Harvesting Applications

B. L. Ooi · **J. M. Gilbert** · **A. Rashid A. Aziz**

Abstract Due to the increasing demand for harvesting energy from environmental vibration, for use in self-powered electronic applications, cantilever-based vibration energy harvesting has attracted great interest from various parties and become one of the most common approaches to convert redundant mechanical energy into electrical energy. As the output voltage produces from a piezoelectric material depends greatly on the geometric shape and the size of the beam, there is a need to model and compare the performance of cantilever beams of differing geometries. This paper presents the study of strain distribution in various shapes of cantilever beams, including a convex and concave edge profile elliptical beams that have been overseen in most of the prior literature. Both analytical and finite element models are derived and the resultant strain distributions in the beam are computed based on MATLAB solver and ANSYS finite element analysis tools. An optimum geometry for a vibration-based energy harvester system is verified. Lastly, experimental results comparing the power density for a triangular and rectangular piezoelectric beams are also presented to validate the finding of the study and the claim as suggested in the literature is verified.

B. L. Ooi
Faculty of Integrative Sciences and Technology,
Quest International University Perak (QIUP),
227 Jalan Raja Permaisuri Bainun,
30250 Ipoh, Perak, Malaysia.
Tel.: +60-012-4366628
E-mail: benglee_85@hotmail.com

J. M. Gilbert
Faculty of Science and Engineering,
School of Engineering, University of Hull,
Cottingham Road, Hull, HU6 7RX, United Kingdom.

A. Rashid A. Aziz
Center for Automotive Research and Electric Mobility (CAREM),
Universiti Teknologi PETRONAS (UTP),
Bandar Seri Iskandar, 31750, Tronoh Perak, Malaysia.

1 Introduction

Energy harvesting is the process by which energy is captured from ambient resources (e.g., solar, thermal, wind, biochemical, vibration and etc.) and converted to electrical energy for storage or use. Over the last decade, due to the advances in integrated circuits, the size and power consumption of electronic devices have been dramatically reduced [1], which has made it possible to power devices by energy harvesting techniques without any external power sources. Wireless sensor systems are creating much interest because of their flexibility and wider range of usable applications. By removing the wire or replaceable battery from the devices, this unlocks the potential for placing the devices in previously inaccessible locations, such as roof tops, underneath floor panels, implanted into building walls etc. On top of this, by incorporating the energy harvesting into devices, several shortcomings of conventional electronic devices may be overcome, such as the limited lifetime that results from the finite batteries capacity and higher maintenance costs for batteries replacement programs.

Vibration energy is one of the common resources that is available at many locations targeted for wireless sensors. For example, vibration energy is generally left unused and redundant in buildings, machinery, traffic infrastructures and many more locations. This makes vibration energy one of the most attractive energy harvesting area to be further investigated for use in electronic devices and wireless sensor networks as the power source. A few different types of transducer are generally used for the conversion of vibration to electricity, they are: electrostatic [2], electromagnetic [3], magnetostrictive [4] and piezoelectric [5]. Each type has its own advantages and drawbacks in term of the device size, output power density, cost and so on. However, due to the energy conversion efficiency, piezoelectric transducers have rapidly gained momentum in recent years as one of the most reliable mechanisms for converting mechanical energy into electrical form [6]. Piezoelectric materials are resilient, chemically inert, small in size and allow operation at high temperature, humidity and other challenging environmental conditions. This makes this type of transducer suitable for many industrial applications, such as powering machinery sensors that operate over a wide temperature range and in dusty environments.

Although there are many other type of beam configurations available [7–10], cantilever beam configurations are still in favor as they give lower resonant frequencies and relatively higher strain for a given force input [11], whereas the successful maximum power harvested has shown to be greater for beams with lower resonant frequencies [12]. An electrical potential difference will be generated from a piezoelectric material when pressure is applied to it. This effect is widely utilized by many researchers in energy harvesting to convert kinetic motions into electrical energy. Many sources in the literature have shown that piezoelectric transduction is an effective conversion mechanism for use in energy harvesting [13–16]. These energy harvesting devices typically consists of a cantilever beam made from a piezoelectric element and a tip mass. Vibration of the mounting of the cantilever causes deformation of the beam and hence the generation of electricity. In order to extract the greatest output voltage from a piezoelectric material, the type of materials and shape of the beam must be carefully selected. Due to its high piezoelectric coupling coefficient, Lead Zicronate Titanate (PZT) is preferable to other materials [17] including Zinc oxide (ZnO), Gallium Orthophosphate (GaPO4) and Polyvinylidene Difluoride (PVDF). Apart from the material, the geometric parameters such as the beam width, thickness and length will also affect on amount of output generating from the beam [18]. To maximize the output, one can matches the electrical circuit impedance to the output load [19], or maximizes the material efficiency by maintaining a higher level of average strain in the beam elements. Yet,
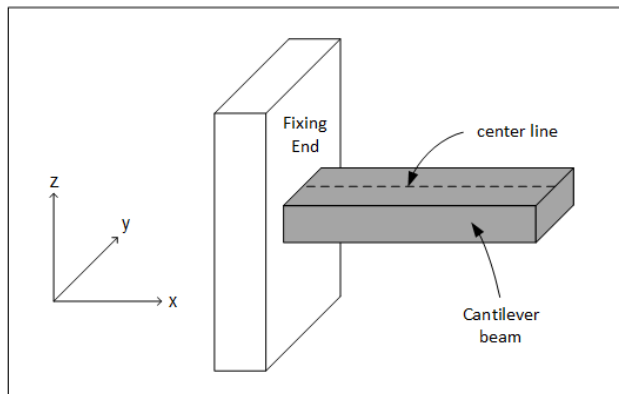
Fig. 1 Center line on a rectangular cantilever beam

the peak strain must be limited to avoid permanent damage to the beam. Thus, the greatest power density can be achieved if all parts of the cantilever experience equal strain at a value just below the maximum acceptable strain on the material (the maximum acceptable strain might be set to the yield strength of the material, or at a lower value selected to give an appropriate number of cycles before failure due to fatigue). Some works have been done to mathematically compare the performance from various shapes of piezoelectric beam [20,21]. It is concluded that, for the same volume of piezoelectric material, a tapered beam (approaching a triangular shape) will have more evenly distributed strain throughout the structure as opposed to a rectangular beam that contains a non-uniform strain distribution. Hence, a smaller, higher average output power density and less expensive harvester can be achieved by implementing a truncated triangle cantilever beam in an energy harvesting system. However, it is worthwhile to investigate the output response and behavior from an elliptically profiled beams which, to author best knowledge, yet to be considered in any previous literature works. It is known that the fundamental vibration frequency for almost all the energy harvester applications is fell under lower frequency, typically from 10 Hz to 250 Hz [22]. Hence, it is assumed that all the beams under investigation in this paper will only be oscillated in 1st mode vibration and due to this assumption, it is appropriate and sufficient to model the beam using static analysis.

The main focus of this paper is to compare the strain distribution of various geometry shapes of single layer cantilever beam, including the elliptically profiled beams. The strain effects in each beam are studied analytically and numerically by using the MATLAB solver and ANSYS multiphysics tools, respectively. Both simulated results are then discussed and benchmarked among themselves to validate the findings in this investigation. Experimental results are also presented to validate the findings from analytical and finite element analysis studies and, lastly, the results are discussed and conclusions drawn.
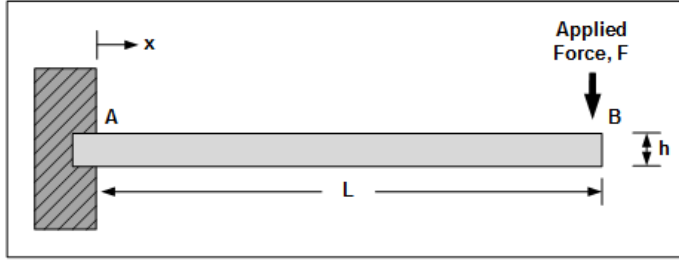
Fig. 2 Cantilever beam with concentrated force at the free end

2 Analytical modelling of a cantilever beam

2.1 Model

An analytical model is developed to determine the strain along the center line of the cantilever in the x direction. It will be assumed that the strain is uniform in the y direction as given in Fig. 1.

For a cantilever beam with one end fixed and the other end is free to move, as shown in Fig. 2, the bending moment, M, at a point x along the cantilever beam from point A to point B, can be given as [23]:

$$M(x) = F(L - x) \tag{1}$$

When the width of the beam, $b(x)$ is allowed to vary along its length, x, the moment of inertia at a distance x from the root is:

$$I(x) = \frac{b(x)h^3}{12} \tag{2}$$

where F is the free end force, x is the position along the beam from the origin point A, L is the total length of the beam, b and h are the width and height dimension of the beam, respectively. Assuming that the strain across the width of the cantilever beam is constant and that the deflection is small, then it is clear that when $x = L$, the bending moment at the free end for the cantilever will becomes zero. Generally, the tensile stress experienced by the beam can be expressed as [23]:

$$\sigma = \frac{M(x)c}{I(x)} = Ec\frac{\partial^2 u}{\partial x^2} \tag{3}$$

where c is the distance from the beams neutral axis to a point of interest (c is constant along x for a fixed height cantilever beam), $\frac{\partial^2 u}{\partial x^2}$ is the second derivative of the beam deflection, u, and E is the Youngs Modulus for the material used in beam. The relationship of bending strain at any x location as a function of beam curvature, R, and the distance from the neutral axis can be given as [24]:

$$\varepsilon(x) = \frac{c}{R} \tag{4}$$

Given that the Youngs Modulus for the material is $E = \sigma/\varepsilon$, then this gives the axial strain above the neutral axis as:

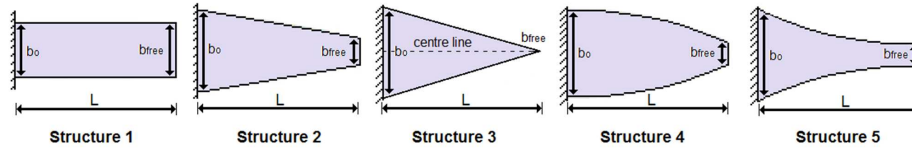$$\varepsilon(x) = c\frac{\partial^2 u}{\partial x^2} = \frac{M(x)c}{IE} \tag{5}$$

Fig. 3 Different geometry shape cantilever beams under investigation

Table 1 Fixed and free end width dimensions for different geometry beam structures

Structures	Fixed end width, b_o (mm)	Fixed end width, b_{free} (mm)
1	10	10
2	15	5
3	15	very small < 1
4	16	4
5	16	4

This implies that the second derivative of the beam deflection is equal to the inverse of the radius of curvature, $\frac{\partial^2 u}{\partial x^2} = \frac{1}{R}$.

Five different geometry beam structures have been investigated under this study, as shown in Fig. 3. Structure 1 is an ordinary rectangular beam, structure 2 is a trapezoidal beam and structure 3 is a triangular beam (ultimate trapezoidal condition). Two elliptically profiled beams were also included in the study to further investigate the effect on the beam strain if the width geometry varies elliptically; they are structures 4 and 5, which have convex and concave edge profile, respectively. If a line along the beam length is drawn through the center line of the beam surface, perpendicular to the fixed end then the strain values at all points on the center line (only shown in structure 3 but applies to all structures in Fig. 3) can be considered and plotted. All structures under test are fixed on one side while a constant tip force is applied at the free end. For the purpose of these calculations, it is assumed that the beam length, L, and height, h (not shown in the figure), are set as 30 mm and 2 mm, respectively. The width dimensions of the beam ends for all the structures under test are summarized in Table 1.

Due to the differences in the beam profiles given Fig. 3, the strains in the beams for a given load is not directly comparable. Hence, to normalize all the relative strain from the different structures, the ratio of relative strain values at each point along the centerline to the maximum strain of that particular structure is considered in the comparison. This is to ensure that all results computed from different geometry structures are normalized and comparable regardless of the differences in geometry parameters. The normalized strain for a given point on the beam can be given as:

$$\varepsilon_n(x) = \frac{\varepsilon(x)}{\varepsilon_m} \tag{6}$$

where x is the position along the beam structure, $\varepsilon(x)$ is the relative strain at position x and ε_m is the maximum relative strain in that particular beam structure. The Eq. 6 is then used as the analytical model to compute the relative strain of the different beam geometries.

2.2 Results and discussion for analytical modelling

In this study, the relative strain on each node is computed analytically based on Eq. 6 and the normalized strains vary along the beam position are given in Fig. 4. It is known that for one to extract the maximum output voltage from piezoelectric materials, the average strain in the entire beam across the width and length must be maximized to the value where the material encounter maximum strain, yet below the material breakage limit that will causes permanent damage to the beam.

For structure 1, an ordinary cantilever beam with rectangular profile, it can be seen that the highest strain concentration is created at the fixed end where the bending moment, M, is at a maximum. However, the strain decreases as the position x along the beam increases, which implies that other than at the fixed end, most of the material elements on this beam are not stress to their limit and hence lower output is expected. Similarly in structure 2, the increasingly triangular trapezoidal profile beam, the highest strain is created at the fixed end and decreases as the beam position increases. However in this structure, the rate of decrease increases until the strain reaches zero at the free end of the beam. Thus, averaged over the length of the beam, this structure will have higher normalized strain in the beam elements as compared to structure 1. For the triangular geometry in structure 3, most of the beam elements are strained to the level that is very close to the material breakage limit and a dramatic decrement occurs only in the region close to the free end of the beam. Hence, this strain energy plot is considered as a close-to-perfect curve since the majority of the material in this beam is stressed to the level just slightly below the material failure limit, which could generates most output for the given volume of material. Furthermore, for the profile of structure 4, the average strain for this beam is slightly greater than the curve as provided by structure 1 but lesser than the ideal curve as provided by structure 3. Lastly, for structure 5, it can be seen that the highest strain concentration is not created at the fixed end like the other four structures under test, but it formed at the intermediate region of the beam length instead. This structure shows a greater average strain curve than any other structures in this study except the profile in structure 3. It is also noteworthy that elliptical beams such as structures 4 and 5 are more complex to fabricate than a trapezoidal beam configurations such as structure 2 and 3. Hence, better average strain curves can be achieved using structure 3 and yet at lower fabricating cost.

Fig. 4 shows the relative normalized strain curves along the center line for various beam profiles. However, it is the volume of material experiencing a particular strain that is of interested. This can be estimated by assigning the normalized strains obtained from the center line of the beam to the entire width of the beam at the particular x value (assuming that the strain across the width of the cantilever beam is constant). Then the general equation of the total nodes available across the beam width at x for those tested structures can be given as:

$$N_b(x) = \frac{b(x)}{b_{free(3)}} \tag{7}$$

where the $b(x)$ is the beam width of the tested structure at x and $b_{free(3)}$ is the free end width in structure 3 (smallest beam width among the structures under test). The particular normalized strain, $\varepsilon_n(x)$, can be obtained by Eq. 6 and the value is then assigned to all the available nodes determined from Eq. 7 for the given x position. By taking the sum of the total nodes available across the beam width for the entire x positions along the cantilever
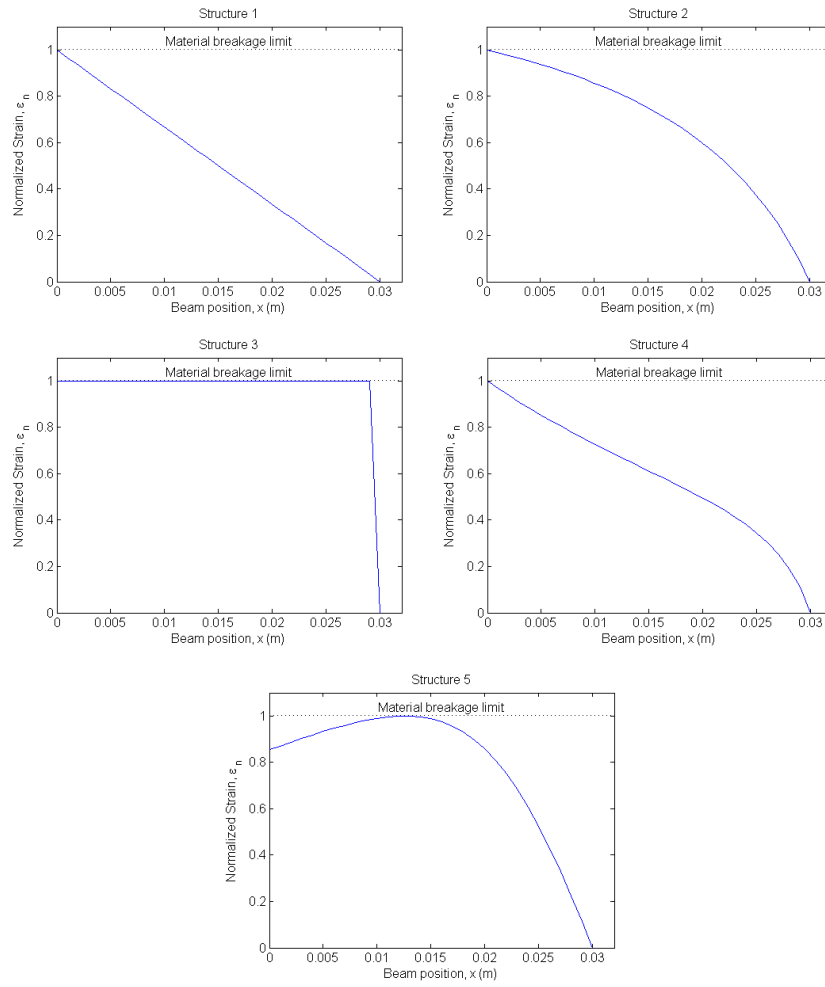
Fig. 4 Normalized strain (analytical) along the center line of various beam shapes under test

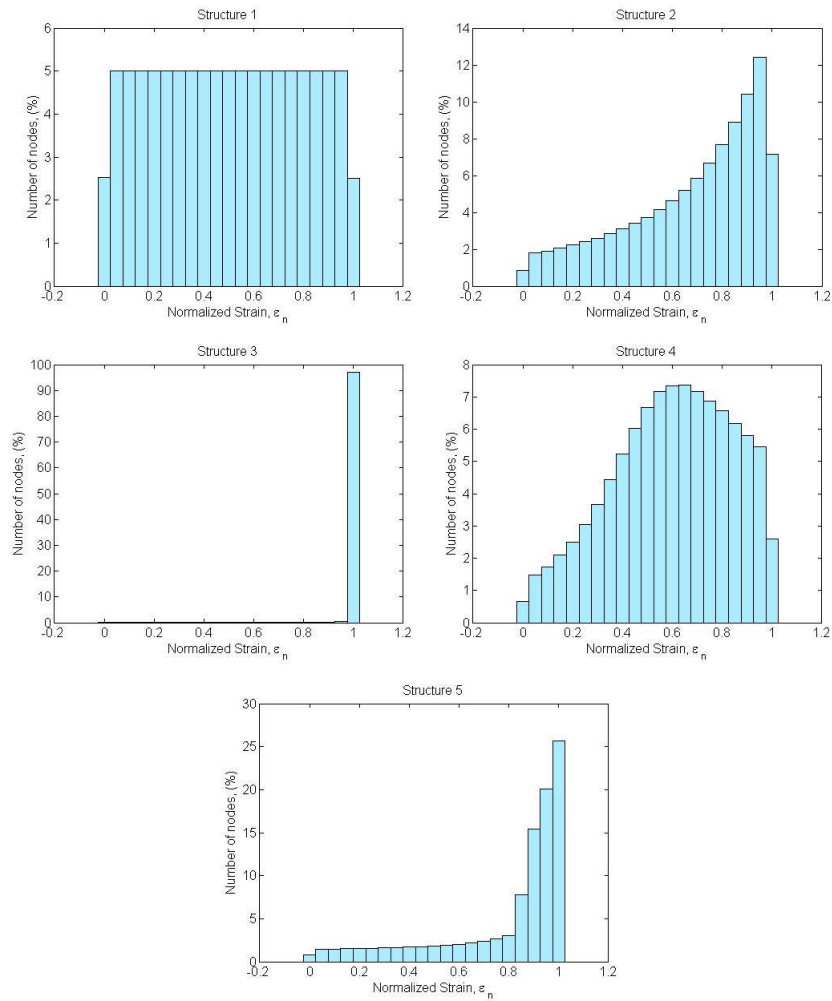length, the total available nodes in a particular structure can be determined by:

$$N_T = \sum_{x=0}^{L} N_b(x) = N_b(0) + \cdots + N_b(L) \tag{8}$$

The values of normalized strain that assigned to all the nodes in the structures may conveniently be visualized as histogram plots with an equally split set of bins. The data is normalized into number of nodes in percentage by $N_{p(\#)} = (N_\#/N_T) \times 100\%$ as given in Fig. 5, where the $N_\#$ is the number of nodes available in that particular bin for $\# = 0, 0.05, 0.1, \ldots 0.95, 1$. The percentage of the nodes for the five structures under test are summarized in Table 2. Only the nodes having the normalized strain that is larger than 0.5 ($N_{p(>0.5)}$) and 0.75 ($N_{p(>0.75)}$) are considered.

From Fig. 5, it can be noticed that structure 1 has almost equal proportion of nodes in each of the bin level, meaning that the structure has non-uniform strain distribution along the

Table 2 Number of nodes with normalized strain (analytical) bigger than 0.5 and 0.75 for beams under test

Structures	Number of nodes with $\varepsilon_n > 0.5$, $N_{p(>0.5)}$ (%)	Number of nodes with $\varepsilon_n > 0.75$, $N_{p(>0.75)}$ (%)
1	50	25
2	84.32	62.44
3	100	100
4	78.15	38.88
5	91.78	85.55

Fig. 5 Histogram plots (analytical) for number of nodes against various values of normalized strain
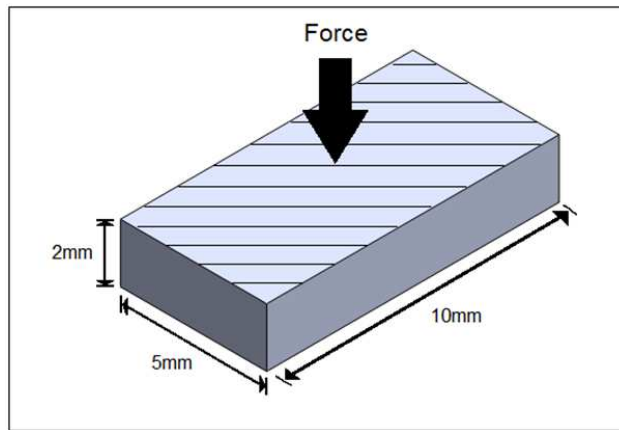
Fig. 6 Tip mass block with a constant force on the striped surface

cantilever beam. Followed by structure 2, the number of nodes increase as the normalized strain goes from lower to higher strain, meaning majority of the available nodes are highly (>0.5) strained in this structure. For structure 3, it shows an almost perfect strain distribution across the beam with almost all the available nodes highly strained at the highest level of the bin. For the elliptical shape structure 4, most of the available nodes are distributed around the middle ranges of the normalized strain. Lastly for structure 5, though most of it available nodes are highly strained, it is still less efficient if compared to structure 3. From Table 2, it clearly indicates that structure 3 gives the best strain distribution among the structures under test in Fig. 3 since the available nodes in this structure are strained at the normalized strain level that is larger than 0.5 and 0.75. Although structure 5 does gives a great strain distribution as compared to structure 1, 2 and 4, this elliptical beam configuration is more difficult to fabricate than structure 2 or 3. Furthermore, structure 3 still provides greater number of nodes that are strained at highest strain level.

3 Finite element modelling of cantilever beam

3.1 Model

In the previous analytical modelling, the strain was assumed to be constant across the width of the cantilever beam, but practically it is not the case. Hence, in this section, modelling has been carried out on similar structures as shown in Fig. 3 using the ANSYS structural static stress analysis tool, to compare the strain distribution for a single layer piezoelectric (PZT-5A4E) cantilever beam. The Youngs Modulus and Poissons ratio for the material used in the beam are given as $66\,\mathrm{Nm}^{-2}$ and 0.31, respectively. Similar to the analytical modelling, all the structures under test are fixed on the left end, but now with the tip mass represented as a block of material $(10 \times 5 \times 2\,\mathrm{mm})$ attached at the free end of the cantilever. A constant force is then applied on the striped surface of the block as illustrated in Fig. 6. All the structures under test are discretized (meshed) with a fix element size of 1 mm in length as depicted in Fig. 7. Lastly, the location of the block of tip mass on each structure is marked with the dashed lines in Fig. 7.
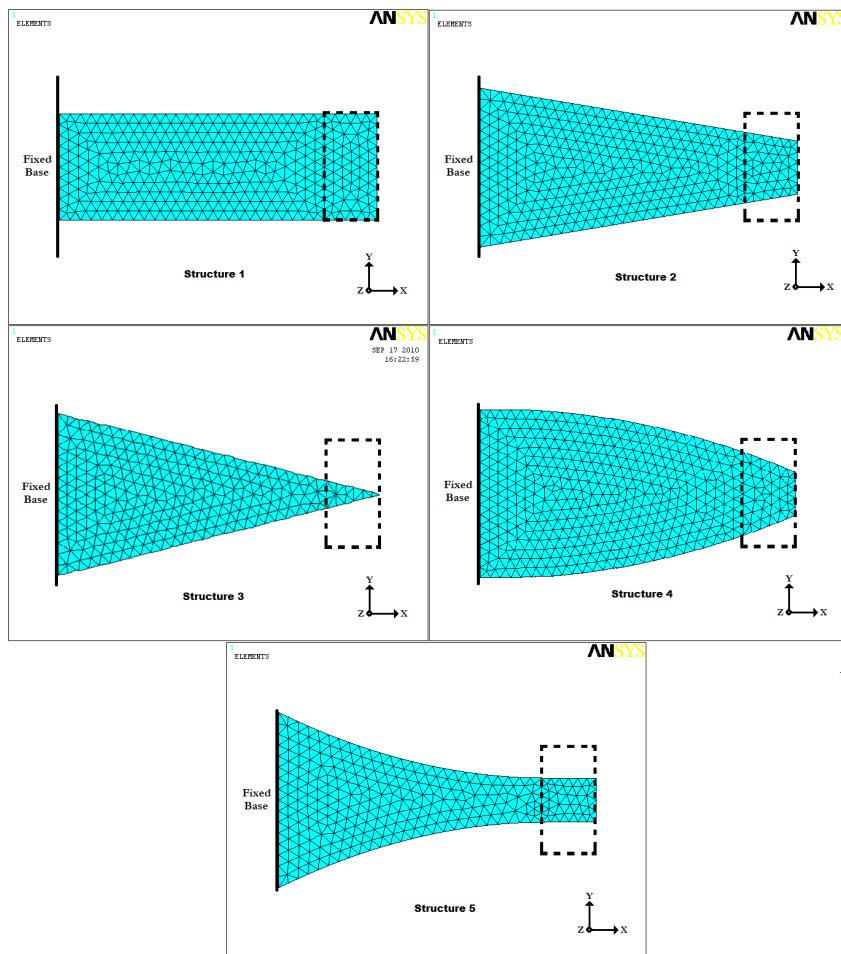
Fig. 7 Discretization of beam structures under test

By applying a fixed force to all the structures on the tip mass which is placed at the free end of each structure, the strain distribution for these beams can be computed by the ANSYS tool as given in Fig. 8. The color tones on each structure indicates the stain level at that particular point. To get a pragmatic strain outputs from these structures, one should carefully selects the applied force so that the highest strain in the material of the structure is limited below the material breakage limit. Due to the fact that the maximum strain for every structure is altered when the geometry has changed, so it is necessary to normalized the strain for a given point obtaining from the beam as according to Eq. 6. The normalization is not only to ensure that all data obtained from various geometries are comparable within this model, but also comparable with those obtained from the previous analytical model as discussed in section 2.
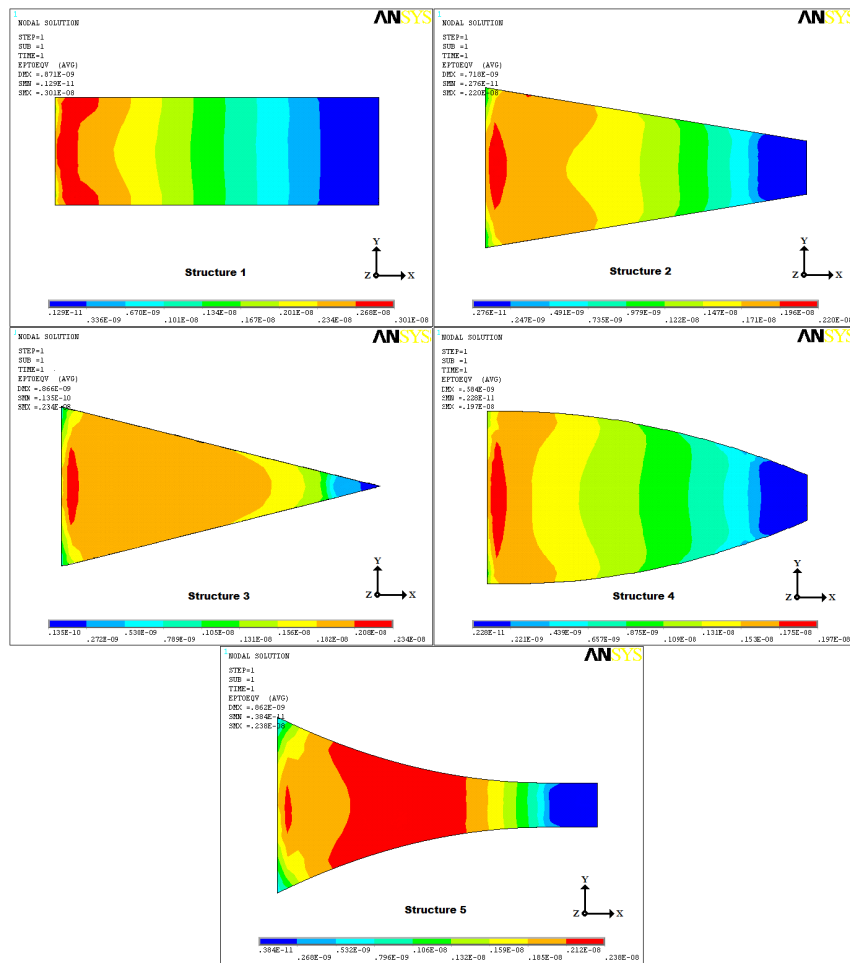
Fig. 8 ANSYS structural analysis of beam structures under test

3.2 Results and discussion for finite element modeling

From Fig. 8, it can be seen that the strain distribution on each structure varies when the beam geometry changes and is not uniform across the beam width, as was assumed in the previous analytical model. However, it is difficult to determine which structure provides the best strain distribution by just observing the color tone (red means highly strained zone, blue means the opposite). Hence, to make this finite element model comparable with the previous analytical model, the relative strain along the beam center line (refer to Fig. 3 and the histogram according to the number of nodes against various values of normalized strain bins are plotted in Fig. 9 and Fig. 10 respectively. Due to the fact that the strain across the width of the cantilever is no longer constant in each geometry, as computed by ANSYS analysis, the data show in Fig. 9 and Fig. 10 are more variable than those obtained from analytical model and shown in the Fig. 4 and Fig. 5.
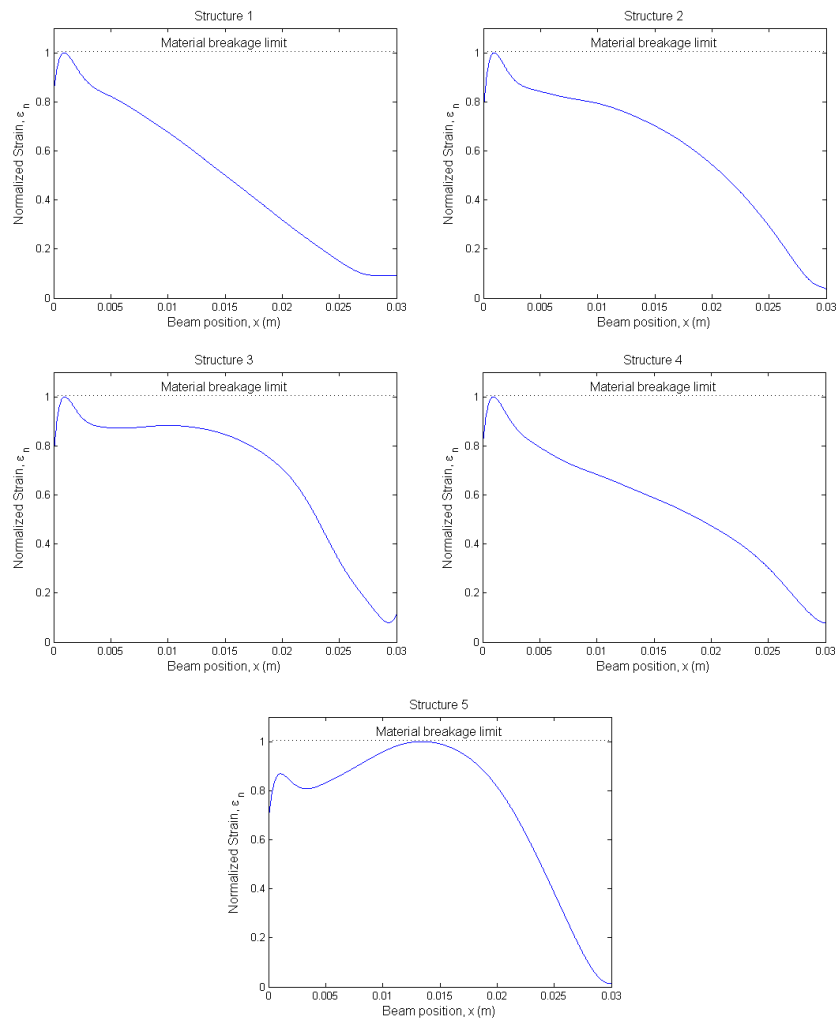
Fig. 9 Normalized strain (finite element) along the center line of various beam shapes under test

Despite the variability of the data from structural analysis, both finite element analysis and analytical data are similar in the sense of their behavior. The trend of the curves in Fig. 9 and the histogram plots in Fig. 10 can be compared with those obtained analytically in Fig. 4 and Fig. 5. It can be noticed that in this strain distribution study, the ANSYS structural study is a more precise model which considered all the non-uniform strain distribution in each structure as compared to the analytical model computed by MATLAB solver, which assumed that strain are constant across the width of the beam length. Although it is mathematically possible to model the strain distribution without making any constant strain assumption analytically, this would add complexity to the calculation in the model and the ANSYS structural analysis method may be considered to be more effective and less time consuming.

From the data given in Fig. 8, it can be seen that there are regions of beam material that are highly strained at the positions next to the fixed end in each structure. Similarly
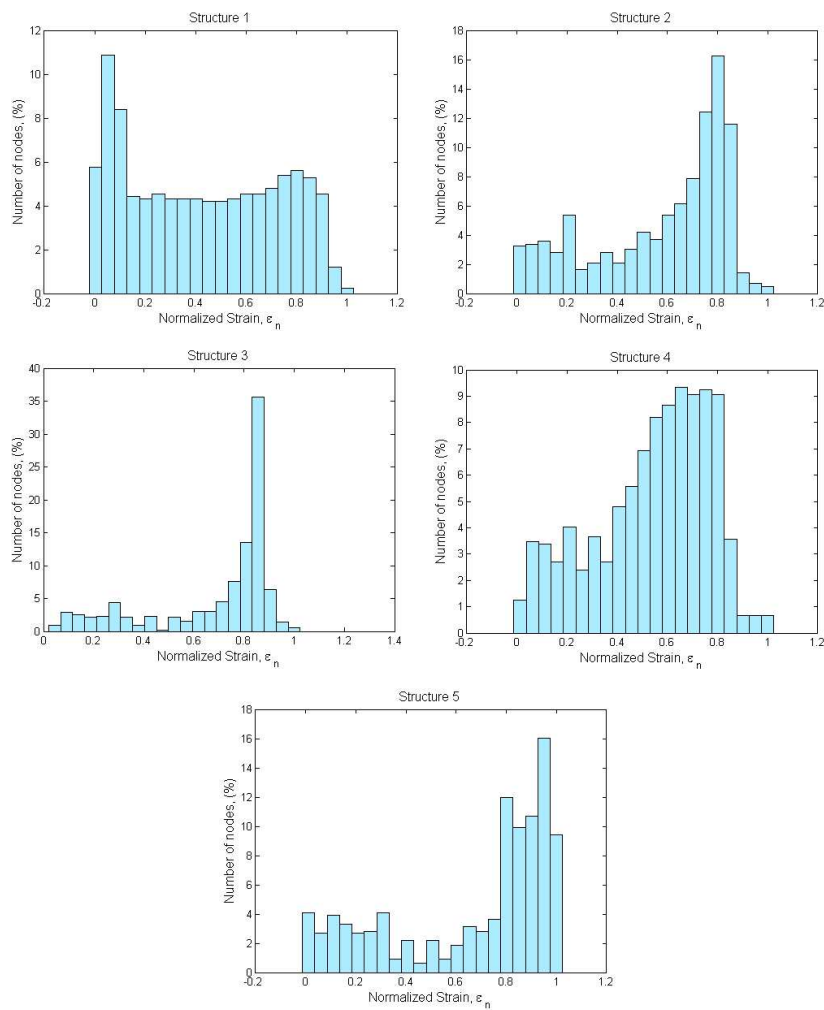
Fig. 10 Histogram plots (finite element) for number of nodes against various values of normalized strain

in Fig. 9, the normalized strain plots shown that all the structures under test have a spike at approximately beam position $x \approx 1\,\text{mm}$, which implies high stress concentration at that beam section. Practically, this has reduced the maximum strain which can be allowed to be applied on each structure before the material breakage limit. In structure 5, the stress concentration at the middle section of the beam seems to be higher than the one near to the fixed end section, however this kind of strain distribution pattern will result in beam failure if an average strain of the beam is the main concern as the strain in the beam goes beyond the material breakage limit if the average strain is pushed to the limit.

Similarly to the analytical model, the percentage of the nodes that have normalized strain that is larger than 0.5 ($N_{p(>0.5)}$) and 0.75 ($N_{p(>0.75)}$) in the five structures under test are summarized in Table 3. Although the overall percentages shown in this table are lower than those in Table 2, they are similar in the sense of their behavior. From Fig. 9 and Fig. 10,

Table 3 Number of nodes with normalized strain (finite element) bigger than 0.5 and 0.75 for beams under test

Structures	Number of nodes with $\varepsilon_n > 0.5$, $N_{p(>0.5)}$ (%)	Number of nodes with $\varepsilon_n > 0.75$, $N_{p(>0.75)}$ (%)
1	42.35	20.10
2	68.45	38.28
3	79.33	63.37
4	63.23	19.54
5	72.01	60.06

it can be noticed that structure 5 is comparable with structure 3 in terms of their average strain in the beam. However from Table 3, it clearly indicates that structure 3 still gives the best average strain distribution according to the percentage of the nodes. It consists of 79.33 % of the nodes that having normalized strain which is larger than 0.5 and 63.37 % of the nodes that having the normalized stain which is larger than 0.75. This clearly justified that structure 3 is still the most efficient structure to maintain optimum average strain in the material across the beam. Not to mention that it is also more cost effective to fabricate a triangular structure than an elliptical beams structure that could come with various elliptical geometry profiles.

4 Experimental results

According to both aforementioned analytical and finite element model outputs, it verifies that structure 3 is the most highly strained and cost effective geometry to be used in piezo-electric cantilever-based energy harvesting system. Due to the good agreement between the analytical and finite element outputs, this justify the reliability of both of the models. Apart from that, it is also costly and difficult to cut the piezoelectric material manually into an elliptical shape without breaking the piezoelectric elements. Piezoelectric material is best cut using a special diamond saw, however even with practice this method does still yield destructive cut to the parts which may affect the behavior of the beam entirely. Hence, in this section, only an actual output power from a conventional rectangular beam (structure 1) will be compared with the output from a triangular beam (structure 3) and it is believed that the validation for other structures are sufficient enough from the models.

The piezoelectric bimorph actuators from Piezo System Inc. are used in this experiment. Each beam consists of a layer of brass sandwiched between layers of PZT-5A4E material. Fig. 11 shows the rectangular bender beam and a smaller bender beam that is carefully cut into a triangular shape from a square beam. The control system setup for this experiment is shown in Fig. 12. Both beams were mounted on a vibration shaker (LDS-V406/8) which was driven by a range of driving frequencies from 40 to 60 Hz at acceleration amplitude of 0.5 g. To determine the available maximum power that will be delivered to the load, both beam outputs were connected to their optimum matched resistance, which were experimentally determined as 71 $k\Omega$ and 22 $k\Omega$ for the triangular and rectangular benders respectively. The outputs from the prototypes were recorded and analyzed by using a data acquisition adapter (ADLINK DAQ-2205). The generated power was then computed as $P = V^2/R$, where V is the peak voltage transferred to the resistive load for the system R, and the output response of the power against the sweep driving frequencies is plotted as in Fig. 13.
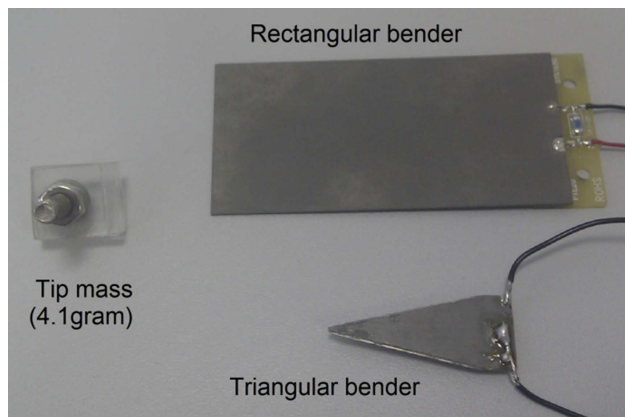
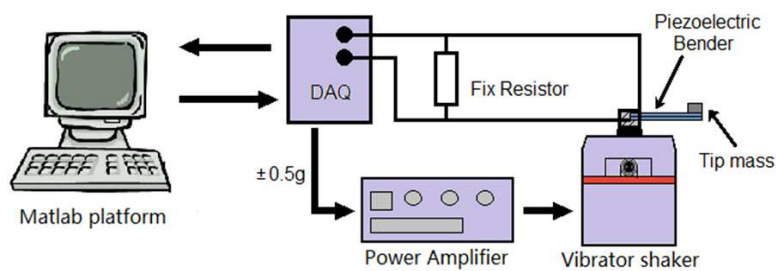**Fig. 11** Rectangular and triangular geometry benders

Fig. 12 Experimental setup of a vibration shaker system

Fig. 13(a) illustrates the recorded outputs from both triangular and rectangular beams. It indicates that the maximum power recorded from the rectangular beam is higher than the output recorded from the triangular beam. The rectangular and triangular beams produce 1.58 mW at 43.7 Hz and 0.23 mW at 45.5 Hz respectively, which is contrasting with the finding in the aforementioned analytical and finite element models, that suggesting a triangular beam is a better beam structure for energy harvesting system. However, this contrast is mainly due to the difference in the size of the piezoelectric bimorph actuators used in the experiment. Comparing the power density for the two cantilevers, which have effective material volumes of $721.7\,\text{mm}^3$ ($44.5 \times 31.8 \times 0.51$ mm) and $56.1\,\text{mm}^3$ ($1/2 \times 20 \times 11 \times 0.51$ mm), respectively, produces the frequency responses shown in Fig. 13(b). After normalizing the output power, the triangular beam is seen to record a higher output power density than the rectangular beam. The peak normalized power densities (NPD) are obtained as $2.19\,\mu\text{W/mm}^3$ and $4.05\,\mu\text{W/mm}^3$ for the rectangular and triangular beam respectively, which is agree with the finding of the analytical and finite element models, triangular beam will produces higher output power than the rectangular beam. To further clarifying the comparison, Table 4 is created to summarize the maximum output power, beam volume and normalized power density (NPD) of both beams under test in this experiment. Roundy et al. [11] claimed that with the same volume of PZT and an increasingly triangular trapezoidal profile to the beam, the strain distribution can be made more even. Hence, an ultimate trapezoidal geometry (triangle) beam can produce twice the power (per unit volume of PZT) than the conventional rectangular geometry beam. However, less than twice energy was obtained

Table 4 Summary of comparison between triangular and rectangular beams

Shape	Maximum Output Power (mW)	Volume (mm³)	Normalized Power Densities (NPD, μW/mm³)
Rectangular	1.58	721	2.19
Triangular	0.23	56.1	4.05
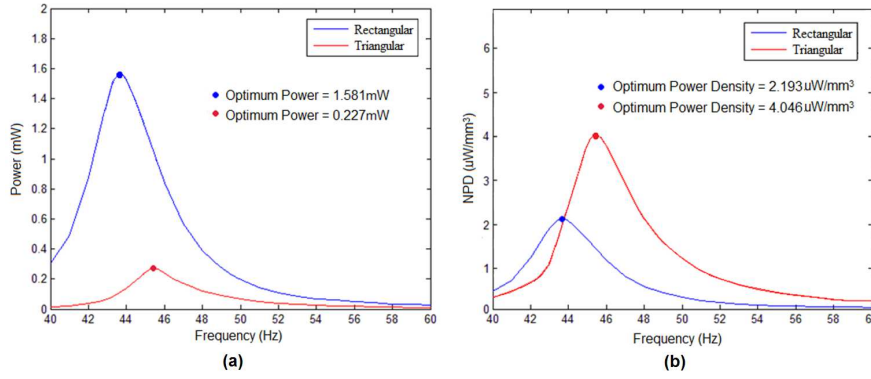
Fig. 13 Comparison of output from rectangular and triangular beam (a) initiate and (b) normalized output power

in this experiment $(4.05/2.19 = 1.85)$. This may be caused by the imperfection of the triangular profile of the structure during the shearing process, which was completed manually instead of using machine cutting.

5 Conclusion

This paper presents the strain distribution analysis of five cantilever structures that come with different geometric configurations, including an elliptically profiled beams that never been considered in any prior literature. Analytical and finite element models of the structures under test are implemented in MATLAB solver and ANSYS finite element analysis respectively. All the strain values on the investigated nodes from each structures are computed and normalized so that the results obtained from different set of models can be compared and the structure with a greater average strain can be determined. The results recorded from both models are comparable in the sense of the behavior: both models suggested that a triangular shape (structure 3) cantilever beam is the best geometry to improve the output power for vibration-based energy harvester. The triangular structure not only maximizes the material average strain for a given input, but also improves the robustness by reducing stress concentration on the cantilever beam. With this improvement, both size and cost of a system can be greatly reduced. Although the results show that a concave elliptical profiled beam (structure 5) look very promising in term of its output power as compared to any other structures under tested, numerical tabulation still conveys that structure 3 gives the best average strain distribution according to the percentage of the nodes, thus filling a gap in the literature to conclude that triangular beam is still better than an elliptical profiled beams that yet to be considered in any of the previous studies. Not to mention the cost to fabricate a triangular structure can be relatively lower as compared to an elliptical beams structure shape that is more complex.

Lastly, this finding is also supported by the experimental outcome, which clearly proved that a triangular geometry can definitely produces greater power density (NPD) than the ordinary rectangular geometry. There is roughly 85 % of power density improvement recorded from the triangular beam as compared to the conventional rectangular beam, due to a greater average strain in the beam material.

References

 1. L. Tang, Y. Yang, C.K. Soh, Journal of Intelligent Material Systems and Structures **21**(18), 1867 (2010). DOI 10.1177/1045389X10390249
 2. S. Meninger, J.O. Mur-Miranda, R. Amirtharajah, A.P. Chandrakasan, H.J. Lang, IEEE Transactions on Very Large Scale Integration (VLSI) Systems, **1**, 64 (2001)
 3. B.L. Ooi, J.M. Gilbert, Sensors and Actuators, A: Physical **213**, 9 (2014). DOI 10.1016/j.sna.2014.03.037
 4. L. Wang, F.G. Yuan, Smart Materials and Structures **17**(4), 45009 (2008)
 5. W. Wang, R.J. Huang, C.J. Huang, L.F. Li, Acta Mechanica Sinica **30**(6), 884 (2015). DOI 10.1007/s10409-014-0115-9
 6. S. Priya, D.J. Inman, *Energy harvesting technologies* (Springer US, 2009). DOI 10.1007/978-0-387-76464-1
 7. H. Hu, H. Xue, Y. Hu, IEEE Transactions on Ultrasonics, Ferroelectrics and Frequency Control **54**(6), 1177 (2007). DOI 10.1109/TUFFC.2007.371
 8. Y. Jeon, R. Sood, J.h. Jeong, S.G. Kim, Sensors and Actuators A: Physical **122**(1), 16 (2005). DOI 10.1016/j.sna.2004.12.032
 9. M.A. Karami, D.J. Inman, Journal of Microelectromechanical Systems **21**(1), 145 (2012). DOI 10.1109/JMEMS.2011.2171321
10. Y. Shindo, F. Narita, International Journal of Mechanics and Materials in Design **10**(3), 305 (2014). DOI 10.1007/s10999-014-9247-0
11. S. Roundy, E.S. Leland, J. Baker, E. Carleton, E. Reilly, E. Lai, B. Otis, J.M. Rabaey, P.K. Wright, V. Sundararajan. Improving power output for vibration-based energy scavengers (2005). DOI 10.1109/MPRV.2005.14
12. S. Jiang, X. Li, S. Guo, Y. Hu, J. Yang, Q. Jiang. Performance of a piezoelectric bimorph for scavenging vibration energy (2005)
13. R. Ly, M. Rguiti, S. DAstorg, A. Hajjaji, C. Courtois, A. Leriche, Sensors and Actuators A: Physical **168**(1), 95 (2011). DOI 10.1016/j.sna.2011.04.020
14. C. Pan, Z. Liu, Y. Chen, Current Applied Physics **12**(3), 684 (2012). DOI 10.1016/j.cap.2011.10.005
15. H. Shen, H. Ji, J. Qiu, Y. Bian, D. Liu, Sensors and Actuators A: Physical **226**, 21 (2015). DOI 10.1016/j.sna.2015.02.008
16. C.K. Thein, B.L. Ooi, J.S. Liu, J.M. Gilbert, Journal of Engineering Science and Technology **(In Press)** (2015)
17. A.G. Muthalif, N.D. Nordin, Mechanical Systems and Signal Processing **54-55**, 417 (2015). DOI 10.1016/j.ymssp.2014.07.014
18. M.I. Friswell, S. Adhikari, Journal of Applied Physics **108**(1), 014901 (2010). DOI 10.1063/1.3457330
19. A.A. Basari, S. Awaji, S. Wang, S. Hashimoto, S. Kumagai, K. Suto, H. Okada, H. Okuno, B. Homm, W. Jiang, S. Wang, Journal of Power and Energy Engineering **02**(09), 117 (2014). DOI 10.4236/jpee.2014.29017
20. S.B. Ayed, F. Najar, A. Abdelkefi, in *2009 3rd International Conference on Signals, Circuits and Systems (SCS)* (IEEE, 2009), pp. 1–6. DOI 10.1109/ICSCS.2009.5412553
21. L. Mateu, F. Moll, Journal of Intelligent Material Systems and Structures **16**(10), 835 (2005). DOI 10.1177/1045389X05055280
22. S. Roundy, Energy scavenging for wireless sensor nodes with a focus on vibration to electricity conversion. Ph.D. thesis (2003)
23. P.P. Benham, R.J. Crawford, C.G. Armstrong, *Mechanics of Engineering Materials*, 2nd edn. (Prentice Hall, 1996)
24. M. Negahban. Pure Bending (2000)